## References

[1] Coleman, R.P., "Theory of Self-Excited Mechanical Oscillations of Helicopter Rotors with Hinged Blades," NACA 1351, 1958.

[2] Hohenemser, K.H. and Yin, S-K., "Some Applications of the Method of Multiblade Coordinates," *Journal of the American Helicopter Society,* Vol. 17, July 1972, pp. 3-12.

[3] Biggers, J.C., "Some Approximations to the Flapping Stability of Helicopter Rotors," *Journal of the American Helicopter Society,* Vol. 14, Oct. 1974, pp 24-33.

[4] Gaonkar, G.H. and Peters, D.A., "Flap-lag Stability with Dynamic Inflow by the Method of Multiblade Coordinates," AIAA/ASME/ASCE/AHS 20th Structures, Structural Dynamics, and Materials Conference, St. Louis, Mo., AIAA Paper 79-0729, April 1979.

[5] Gaonkar, G.H. and Peters, D.A., "Use of Multiblade Coordinates for Helicopter Flap-lag Stability with Dynamic Inflow," *Journal of Aircraft,* Vol. 17, Feb. 1980, pp. 112-118.

[6] Hodges, D.H., "Aeromechanical Stability of Helicopters with a Bearingless Main Rotor-Part I: Equations of Motion," NASA TM 78459, 1978.

[7] Briczinski, S.J. and Cooper, D.E., "Flight Investigation of Rotor/Vehicle State Feedback," NASA CR-132546, 1975.

[8] Gaonkar, G.H., "A General Method with Shaping Filters to Study Random Vibration Statistics of Lifting Rotors with Feedback Controls," *Journal of Sound and Vibration,* Vol. 21, No. 2, 1972, pp. 213-225.


AIAA 80-1157R

# Aircraft Engine Combustor Casing Life Simulation Evaluation

S.A. Cimorelli*
*General Electric Aircraft Engine Group, Lynn, Mass.*

## Introduction

A COMBUSTOR casing was tested at room temperature under cyclic pressure conditions to investigate: 1) the nature, location, and orientation of life-limiting defects and/or stress concentrations (weld offset mismatch, reinforcement, and the role of bosses); 2) the feasibility of predicting the component life from existing test specimen data; and 3) the stress distribution and the nominal stress range effective for life analysis at the maximum operative pressures.

The need for a component test was also prompted by the fact that fatigue crack growth in the vicinity of welded joints (let alone crossed welds) is complicated, not only by the stress concentrations due to weld geometry effects (mismatch, offset, etc.), but also because the crack may successively enter layers that differ significantly in their crack growth resistance. This clearly leads to a crack-path dependence of the predicted component life. In this case, the total course of a crack must be either known or predictable in order to integrate life increments by fracture mechanics methods. This, in turn, requires rigorous knowledge of the stress and defect distributions in critical areas. In the lack of such a detailed knowledge of stress distributions and defect populations, life analysis often resorts reasonably to the weakest link concept, which assumes that the crack will grow along, or ultimately "seek," the weakest plane in the weld.

Presented as Paper 80-1157 at the AIAA/SAE/ASME 16th Joint Propulsion Conference, Hartford, Conn., June 30-July 2, 1980; submitted Aug. 22, 1980; revision received Nov. 18, 1980. 

*Engineer, Experimental Mechanics.

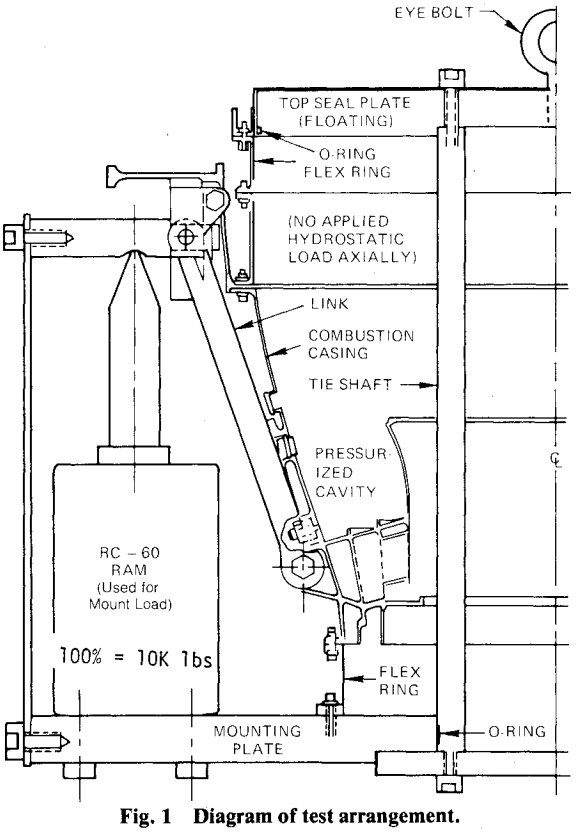


**Fig. 1 Diagram of test arrangement.**

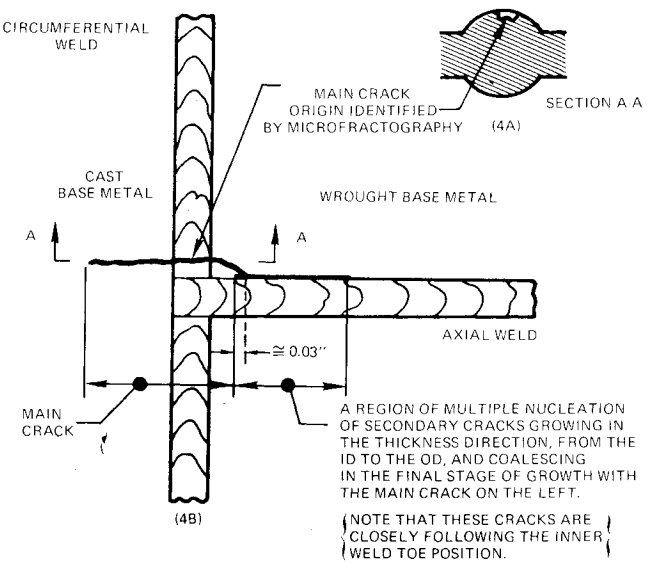


**Fig. 2 A schematic illustration of the crack path in the combustor casing test (i.d. face in plane).**

**Table 1 Crack growth history**

| Cycles | Crack length, in. Fwd | Aft | Total |
|---|---|---|---|
| 250 | | | 0.190 |
| 1500 | 0.058 | 0.062 | 0.280 |
| 2000 | 0.070 | 0.085 | 0.315 |
| 3000 | 0.115 | 0.125 | 0.400 |
| 4000 | 0.150 | 0.160 | 0.460 |
| 4500 | 0.155 | 0.200 | 0.515 |
| 5000 | 0.225 | 0.400 | 0.785 |
| 5500 | 0.250 | 0.425 | 0.835 |
| 6000 | 0.310 | 0.500 | 0.968 |
| 6200 | 0.380 | 0.700 | 1.24 |
| 6500 | 0.500 | 0.850 | 1.51 |
| 6600 | 0.510 | 0.925 | 1.6 |

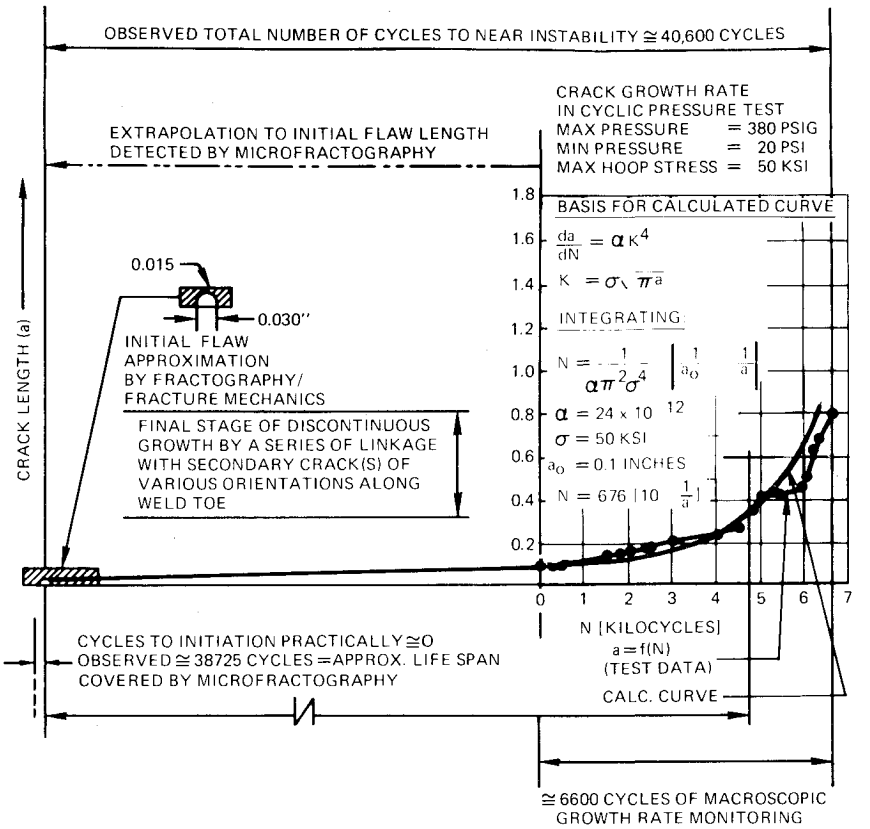


**Fig. 3 Identification of various stages of crack growth monitored both macroscopically and microscopically.**

## Experimental Details Summary

### A. Test Criteria

To insure correct stress distribution it was necessary to simulate the engine assembly regarding flexibility and restraint of flange connections and to be able to provide radial pressure and axial loads that exist during engine operation. The test arrangement included: the combustion chamber, the engine aft mount with the drag link assembly, the mount ring, and the high pressure turbine casing. They were assembled as shown schematically in Fig. 1.

A brittle coating was applied to the entire outside surface between the combustor casing mounting flanges after the test arrangement was assembled. The brittle coating threshold stress was 30 ksi (estimated accuracy ±5 ksi). The casing was hydraulically pressurized in seven equal steps to 252 psig (70% of maximum operating pressure), at which pressure adequate strain patterns were available for strain gage locations and orientations. Twenty strain gages (15 externally and 5 internally) were installed and a stress test was conducted to evaluate the high stress areas.

### B. Stress Range and Stress Distribution

The nominal hoop stress in the skin (away from the welds) was about 50 ksi, whereas strain gages placed directly on the welds showed evidence of local stresses as high as 78 ksi (at the high point of weld reinforcement). Maximum recorded stress was 93 ksi near a boss.

Since the resulting crack was of the axial orientation, our calculations, based on the remote nominal stress, will make use of $\Delta\sigma(0\text{-}\sigma_{max}) \cong$ 50 ksi. This corresponds to a maximum cyclic pressure on the order of 360 psig. A value of $R = \sigma_{min} / \sigma_{max} \cong 0$ can be reasonably assumed in the present analysis, since the minimum pressure was ≤ 20 psig.

The room temperature test parameters were scaled up from high temperature data at 920°F (service temperature).

### C. Cyclic Test

After the completion of the stress tests the combustor casing underwent hydrostatic pressure cycle testing to monitor crack initiation and crack growth rate. It was cycle tested to 360 psig, and periodically inspected for cracks, up to 26,000 cycles. The pressure was then raised to 380 psig and after 8000 more cycles a through crack (≅ 0.18 in.) was observed at the circumferential weld as shown in Fig. 2.

### D. Crack Growth Macromeasurements

After the initiation of a through crack the combustor casing test arrangement was dismantled. The crack was located internally and inspected. A patch about 4 in. in diameter and 0.1 in. thick was applied all around the crack on the inside. GE-RTV was used as the patch. There was some concern that the "rubbery" material would be pushed through the crack at the higher pressures but it was tried anyway. The RTV was not pushed through the crack and the crack growth measurements were made with only the care needed to use a telemicroscope. The use of the patch allowed us to make macromeasurements of the crack during the test, under full pressure, without getting any leakage. Also, the dry exterior surface permitted the use of zyglo penetrant for a better definition of the crack. Further, due to the flexible composition of the patch, there was no effect on the hoop stresses in the wall of the combustor casing. After about 6600 more cycles a crack of 1.6 in. was measured. The crack growth history during the macroscopic study is given in Table 1 (also see Fig. 3).

The total crack growth rate was much faster than expected and there was no macroscopic history before the 0.18 in. through crack so the combustor casing was sent for metallurgical investigation. Accuracies in the test were

Length = ±0.005 in.
Pressure = ±5 psig
Load = ±3% lb
Cycles = ±1.0 cycles
Stress = ±3% psi

The intricate details of the initial flaw shape can be ignored in the first approximation, expecially since, upon incipient growth, the crack rapidly attains a stable configuration (normally semicircular, semielliptic, etc., depending on the stress distribution).

Figure 3 shows an extrapolation of the macroscopic crack length record, $a=f(N)$, over the life span preceding the macroscopic observations, down to a semicircular initial flaw length shown at the start of the cycling curve. Note that this is merely for illustration as the extrapolated $X$ axis in Fig. 3 is not to scale. A median curve drawn through the macroscopic crack growth record, $a=f(N)$ with $a>0.1$ in., was differentiated graphically yielding $da/dN=f_1(a)=f_2(\Delta K)$, which can be plotted against the corresponding $\Delta K$ levels given by

$$\Delta K=\Delta\sigma\sqrt{\pi a} \tag{1}$$

### Acknowledgments

Tests were performed by J.F. Smith Jr., Analyst; and consultation was given by J. Miller, Senior Engineer, Experimental Mechanics Lab, G.E.-AEG, Lynn, Mass.

AIAA 81-4192

# Radar Ranges for Carrier-Based AEW Aircraft

Ralph R. Nebiker*
*Carrier Airborne Early Warning Squadron 115, U.S. Navy, San Francisco, Calif.*

## Introduction

THIS Note describes a simple geometrical model that may be used to examine the affects of various parameters on the minimum required radar range for carrier-based airborne early warning (AEW) aircraft. The motivation for this Note was the work described in Ref. 1, which examined the AEW aircraft in a coastal defense role. Here the development and results are focused on the geometry of an aircraft carrier battle group (BG) at sea (airbase and target colocated), the standoff weapon capability of enemy air-to-surface antiship missiles, and two BG response options with deck-launched interceptors (DLI) and barrier combat air patrol (BARCAP) prepositioned on station.

## Model Development

Figure 1 depicts the basic scenario with the BG at point $A$ and the AEW aircraft at point $B$. Continuation of line $AB$ forms the threat reference axis (TRA) from which significant angles are measured. Attacking fighters need arrive only within distance $L_1$ (the lethal range of their air-to-air weapons) of the AEW aircraft, and attacking bombers need arrive only within distance $W$ (launch range of their antiship missiles) of the BG. The objective is to destroy the bombers before they launch their missiles. The BG commander can, in response, launch DLI from point $A$ or provide BARCAP on station at point $G$. The DLI and BARCAP are equipped with air-to-air weapons of range $L_2$ and fly at velocity $V_4$. If the AEW aircraft pilot decides after a time $T_1$ that he is under attack by enemy fighters, he flees toward point $A$ at velocity $V_3$. The BARCAP is assigned a similar maneuver and decision delay time of $T_2$.

Figure 2 (top) depicts the geometry of a BARCAP interdicting a bomber attack. Let $J$ denote the desired intercept point on the straight-line path $AL$ of the attacking bombers, $X=$ distance $AJ$. With $T=$ the time to engagement,

$$V_4\cdot(T-T_2)+L_2=GJ$$

By the law of cosines

$$GJ^2=S^2+X^2-2\cdot S\cdot X\cdot\cos(A_3-A_2)$$

and

$$T=\frac{[S^2+X^2-2\cdot S\cdot X\cdot\cos(A_3-A_2)]^{1/2}+V_4\cdot T_2-L_2}{V_4} \tag{1}$$

If $|(A_3-A_2)|$ is less than 90 deg *and* $W$ is less than $S\cdot\cos(A_3-A_2)$, then the shortest route to interdiction is $GJ$ perpendicular to $AL$, where $X=S\cdot\cos(A_3-A_2)$; otherwise, $X=W$. To insure sufficient time for intercept $AL=V_1\cdot T+X$ and from triangle $ABL$, where $BL=R$, the required radar range,

$$D\cdot\cos(A_3)+R\cdot\cos(A_4)=V_1\cdot T+X \tag{2}$$

Triangles $ABK$ and $LBK$ yield

$$\sin(A_4)=(D/R)\cdot\sin(A_3)$$

Since $\cos^2+\sin^2=1$, $\cos^2(A_4)=1-(D^2/R^2)\cdot\sin^2(A_3)$. Substituting into Eq. (2) and solving for $R$ leads to

$$R=\{[X+V_1\cdot T-D\cdot\cos(A_3)]^2+D^2\cdot\sin^2(A_3)\}^{1/2} \tag{3}$$

where $T$ is obtained from Eq. (1).

The geometry of a BARCAP response to a fighter attack on the AEW aircraft is depicted in Fig. 2 (bottom). Using the law of cosines for triangle $ABG$ yields

$$GB^2=D^2+S^2-2\cdot D\cdot S\cdot\cos(A_2) \tag{4}$$

Triangles $ABE$ and $CBE$ provide the following relations:

$$A_5=\arcsin(D\cdot\sin(A_1)/R) \tag{5}$$

$$AC=D\cdot\cos(A_1)+R\cdot\cos(A_5) \tag{6}$$

$$CF=AC-S\cdot\cos(A_2-A_1) \tag{7}$$

Triangles $AGF$ and $CGF$ lead to

$$A_6=\arctan(S\cdot\sin(A_2-A_1)/\mathrm{CF}) \tag{8}$$

$$GC=CF/\cos(A_6) \tag{9}$$

Applying the law of cosines to triangle $CBG$ yields

$$A_7=\arccos\left(\frac{R^2+GB^2-GC^2}{2\cdot GB\cdot R}\right) \tag{10}$$

Let $H$ denote the desired intercept point along the straight-line intercept path $CB$ of the attacking fighter, $X=$ distance $BH$. If $|A_7|$ is less than 90 deg *and* $L_1$ is less than $GB\cdot\cos(A_7)$, then the shortest route to interdiction is $GH$ perpendicular to $CB$, where $X=GB\cdot\cos(A_7)$; otherwise $X=L_1$.

From triangle $GBH$ and the law of cosines

$$GH=[GB^2+X^2-2\cdot GB\cdot X\cdot\cos(A_7)]^{1/2} \tag{11}$$

Received Oct. 6, 1980; revision received Dec. 22, 1980. 

*Operations Officer, Commander, VAW-115. Member AIAA.